Intravoxel incoherent motion perfusion in patients with Moyamoya disease: comparison with ^{15}O-gas positron emission tomography

Shoko Hara[1,2] (iD), Masaaki Hori[2], Ryo Ueda[2,3],
Akifumi Hagiwara[2], Shihori Hayashi[1,4], Motoki Inaji[1,4],
Yoji Tanaka[1], Taketoshi Maehara[1], Kenji Ishii[4], Shigeki Aoki[1]
and Tadashi Nariai[1,4]

Abstract

Background: Intravoxel incoherent motion magnetic resonance imaging (IVIM) enables non-invasive measurement of brain perfusion.

Purpose: To investigate whether IVIM could be used to evaluate the hemodynamic disturbance of Moyamoya disease (MMD) by comparison with the gold-standard ^{15}O-gas positron emission tomography (PET) method.

Material and Methods: Ten consecutive patients with MMD (six women; mean age = 42.8 years) and 10 age-matched healthy controls were evaluated by diffusion-weighted images with 12 different b values in the range of 0–900 s/mm^2 and ^{15}O-gas PET. Tomographic maps of IVIM parameters, perfusion fraction (f), pseudo-diffusion coefficient (D^*), and $f \cdot D^*$, as well as cerebral blood volume (CBV), cerebral blood flow (CBF), and mean transit time (MTT) maps obtained with PET, were normalized and hemispheric gray and white matter values were calculated. IVIM parametric values were compared with PET parameters and with clinically assessed disease severity.

Results: There was significant correlation between D^* and MTT ($r = -0.74$, $P < 0.001$) and between $f \cdot D^*$ and CBF ($r = 0.52$, $P = 0.02$) in the cortical areas. The f values in the white matter were significantly higher in symptomatic MMD patients than in healthy controls ($P = 0.01$).

Conclusion: IVIM may be used to non-invasively investigate cerebral hemodynamic impairment in patients with MMD. Further evaluation is needed to establish IVIM usage in clinical settings.

Keywords

Moyamoya disease, diffusion magnetic resonance imaging, intravoxel incoherent motion imaging, ischemia, cerebral blood flow, positron emission tomography

Introduction

Intravoxel incoherent motion (IVIM) perfusion, proposed by Le Bihan (1), is a technique to visualize blood microcirculation in the capillary networks that uses diffusion-weighted magnetic resonance imaging (MRI) with multiple low b values. The IVIM parameters consist of a perfusion fraction (f), which describes the fraction of incoherent signal that arises from the vascular compartment, and a pseudo-diffusion coefficient (D^*), which macroscopically describes the

[1]Department of Neurosurgery, Tokyo Medical and Dental University, Tokyo, Japan
[2]Department of Radiology, Juntendo University, Tokyo, Japan
[3]Department of Radiological Sciences, Tokyo Metropolitan University, Tokyo, Japan
[4]Team for Neuroimaging Research, Tokyo Metropolitan Institute of Gerontology, Tokyo, Japan

Corresponding author:
Shoko Hara, Department of Neurosurgery, Tokyo Medical and Dental University, 1-5-45 Yushima, Bunkyo-ku, Tokyo 113-8519, Japan.
Email: shara.nsrg@tmd.ac.jp

incoherent movement of blood in the microvasculature compartment. Theoretically, f is assumed to be proportional to cerebral blood volume (CBV), $D*$ is assumed to be proportional to the reciprocal value of mean transit time (MTT), and $f \cdot D*$ (the product of the first two parameters) is considered to be a flow-related parameter that correlates with cerebral blood flow (CBF) (2). Most studies using IVIM have investigated its application in the evaluation of body organs (3–5), but recently an increasing number of studies have focused on its application in the brain (6,7). Although several concerns about this technique exist, brain IVIM perfusion is advantageous over other perfusion methods such as positron emission tomography (PET), dynamic susceptibility contrast (DSC), and arterial spin labeling imaging (ASL) since it does not require the injection of contrast media or radiation exposure, and it is not affected by arterial inputs. Numerous studies have demonstrated the clinical feasibility of IVIM in healthy volunteers (8) and patients with brain tumors (2,7), acute stroke (2), white matter disease (9,10), and brain death (11). However, the verification of IVIM parameters, by comparing them with quantitated perfusion parameters, has not yet been performed. Among the various brain perfusion methods, ^{15}O-gas PET is considered the most reliable technique for quantitation of multiple perfusion parameters (12), such as CBF and CBV; MTT can also be calculated using PET, as CBV/CBF. In the present study, we examined whether IVIM parameters correlate with the quantitated hemodynamic parameters measured using PET in patients with Moyamoya disease (MMD).

MMD is a rare cerebrovascular disease that primarily affects children and young adults (13); it is characterized by progressive occlusion of intracranial major arteries and development of a collateral vascular network. Clinical presentation and hemodynamic conditions of this disease vary greatly across patients (14), presumably due to the variable speed of disease progression and degree of collateral development. Previous studies, using PET (14), DSC (15), and ASL (16), have indicated that CBF, CBV, and MTT of patients with MMD varies across individuals and affected regions. Therefore, patients with MMD are suitable individuals for validating the utility of newly established IVIM parameters, using PET-measured quantitative parameters. It is expected that CBV and MTT would increase and CBF would decrease as the disease burden became severe: accordingly, IVIM of patients with MMD would result in high f values, low $D*$ and low $f \cdot D*$ values, respectively.

The aim of this study is to evaluate whether IVIM parameters correlate with PET-measured true hemodynamic parameters and/or reflects the proposed ischemic burden of MMD.

Material and Methods

Participants

The local ethical committees approved this prospective study and written informed consent was obtained from all participants. From September 2015 to January 2017, 10 patients with MMD recruited to the study (six women; mean age = 42.8 years) were evaluated by MRI protocol, including IVIM, and PET, which we performed only when patients required further detailed examination to confirm a possible surgical indication. Patient characteristics, including stages of the disease (17), Fazekas grade (18), and *p.R4810K* variant of the ring finger 213 gene (19), are summarized in Suppl. Table 1. All patients had a history of ischemic events (either transient ischemic attack or infarction) and none of the patients had previously undergone surgery. The average interval between PET and MRI exams was 10.9 days. The presence of arterial stenotic lesions, infarction, hemorrhage, and white matter T2 hyperintensities were assessed by conventional MRI by the neuroradiologist (MH) with 15 years of clinical experience who was blinded to the clinical history of the patients. Three patients harbored cortical infarctions, while eight patients had white matter T2 hyperintensities. One patient exhibited a left temporal hemorrhagic lesion adjacent to the left lateral ventricle (a scar from a previous intraventricular hemorrhage) and another was found to have a small left-thalamic hemorrhage as an incidental finding. During the same period, 10 volunteers (six women, mean age = 38 years) who were selected to match the age of patients were recruited and evaluated by MRI alone. Based on these assessments and the clinical histories, all hemispheres were categorized as normal (N), asymptomatic (A), or symptomatic (S, with focal ischemic symptoms or infarctions on MRI). All hemispheres of normal controls were categorized as N ($n = 20$), while hemispheres of MMD patients were categorized to either A ($n = 9$) or S ($n = 11$).

MRI acquisition

All MRI data were acquired using a 3-T system with a 32-multichannel receiver head coil (MAGNETOM Skyra, Siemens, Germany). A three-dimensional (3D) T1-weighted (T1W) Magnetization Prepared Rapid Gradient Echo sequence (repetition time [TR]/echo time[TE] =1700/2.61 ms, flip angle = 10°, inversion time [TI] = 800 ms, parallel imaging using GeneRalized Autocalibrating Partial Parallel Acquisition) was acquired for anatomical orientation.

Diffusion-weighted images were acquired using a fat-saturated single-shot echo planar imaging

Table 1. Average values of IVIM parameters.

		Normal (N)		Moyamoya (A+S)		P value
		Mean	SD	Mean	SD	(T test)
Cortex	f (10–2)	6.02	1.05	5.73	0.91	0.35
	D* (10⁻³ mm²/s)	8.23	0.75	7.15	0.14	**<0.001***
	f·D*(10⁻³ mm²/s)	0.18	0.02	0.17	0.02	0.12
	D (mm²/s)	0.53	0.05	0.52	0.07	0.70
	CBV (mL/100 g)	–	–	4.68	0.93	–
	MTT (s)	–	–	6.17	2.07	–
	CBF (mL/min/100 g)	–	–	55.17	14.19	–
White Matter	f (10–2)	8.49	0.83	9.39	0.10	**0.004***
	D* (10⁻³ mm²/s)	9.69	1.14	9.46	0.74	0.44
	f·D*(10⁻³ mm²/s)	0.22	0.01	0.24	0.02	**0.0048***
	D (mm²/s)	0.68	0.01	0.69	0.04	0.27
	CBV (mL/100 g)	–	–	3.12	0.69	–
	MTT (s)	–	–	5.58	1.80	–
	CBF (mL/min/100 g)	–	–	38.20	8.42	–

*$P < 0.05$ and is significant.
SD, standard deviation; N, normal; A, asymptomatic; S, symptomatic (see "Material and Methods" for details).

sequence (TR/TE = 4000/75.4 ms, flip angle = 90°, voxel size = $2 \times 2 \times 2$ mm³, acquisition matrix = 100, number of excitations = 1, number of slices = 78; b-values: 0, 10, 20, 40, 80, 110, 140,170, 200, 300, 600, 900 s/mm², three diffusion-encoding directions, multi-band factor = 2, repetition time = 1). The b-values were determined such that they would increase in an exponential manner from 0 to 900 s/mm². Acquisition time for the diffusion-weighted images was approximately 5 min 48 s, which was within the clinically acceptable scan time. The signal-noise ratio (SNR) at $b = 900$ s/mm² measured in the control white matter of the corona radiata was 31.1 (20), which is larger than the minimum value recommended for accurate IVIM estimation of the f value (8).

IVIM post-processing and computation of parametrical maps

The IVIM parametrical maps were created using the commercially available software, Olea Sphere 3.0 (Olea Medical, La Ciotat, France) (7,21–23), implementing a Bayesian probability-based algorithm (23). The motion correction algorithm achieves pairwise in plane (acquisition plane) rigid co-registration of all diffusion weighted images of a given slice location with a reference image selected by the software algorithm. Software-determined smoothing was added before and after biexponential fitting. The standard IVIM two-compartment diffusion model, with a capillary perfusion component and a non-vascular compartment, was employed. Signal decay was estimated using the biexponential equation described below, on a voxel-by-voxel basis, after averaging the data obtained the three directions of diffusion encoding.

$$\frac{S_b}{S_0} = fe^{-bD^*} + (1-f)e^{-bD}$$

In this equation, S_b and S_0 represent the signal intensity for a given b value and for a b value of 0 s/mm², respectively; f (dimensionless index in the range of 0–1) indicates the relative amount of capillary water in the voxel on the assumption that capillaries are considered in random fashion; and $D*$ (mm²/s) is a perfusion-related component of the signal attenuation mimicking the diffusion process and is dependent on the mean length of the capillary segment and the mean speed of blood-flow. The sum of the squared errors (Chi-square distribution), which represents the fidelity of fitting to the whole brain, in each participant was 1007 (range = 741–1300) on average.

PET acquisition and computation of parametrical maps

The PET data were acquired using a Discovery 710 PET/computed tomography (CT) scanner (GE Healthcare, Milwaukee, WI, USA) (24). After a low-dose CT scan for attenuation correction was performed, 3.5-min emission scans after 1.5-min inhalation of $C^{15}O_2$ (2000 MBq/min) and $C^{15}O$ (2000 MBq/min) were performed with the neck shield in place (25). Levels of radioactivity in arterial blood were manually measured at 0, 2, and 4 min via arterial catheter while images of $C^{15}O_2$ were acquired (26).

The images were reconstructed under the 3D ordered-subset expectation maximization algorithm (128×128 matrix, 47 slices, 2.0 mm/pixel, 3.27 mm/slice, 4 iterations, 16 subsets, and Gaussian filter of 3.0 mm). The clinical $C^{15}O_2$ image consisted of 12 frames of 5 s and 10 frames of 15 s, and the attenuation was corrected using the corresponding CT image. The scatter correction algorithm used a scatter limitation correction. We calculated CBF and CBV from the collected images and amounts of radioactivity in arterial blood using the PET autoradiographic method, with Xeleris software (GE Healthcare) (27). The final spatial resolution of CBF and CBV maps was 5.78 mm.

Processing of parametrical maps

Processing of all parametrical maps was performed in MATLAB 2016a (MathWorks Inc., Natick, MA, USA) and SPM12 (http://www.fil.ion.ucl.ac.uk/spm/), visually summarized in Suppl. Fig. 1. First, the voxels with values < 0 in the f and D^* maps were determined to be non-physiological and were set to 0 (2,28). To eliminate the extremely high signals produced by the large veins and sinuses in the CBV map, the top 0.8% of all values in each map was deleted so as not to be included in the subsequent regional value analysis.

The threshold was empirically decided during this study by visual inspection of the CBV maps. The $f \cdot D^*$ and MTT (CBV/CBF) were then estimated by voxel-by-voxel based calculation. All IVIM and PET parametrical maps were co-registered to the T1W images of each patient. Noise signals in the extra-axial cerebrospinal fluid (CSF) space of the IVIM maps were carefully eliminated using a mask of brain parenchyma created from the b0 image of each patient. A Gaussian smoothing operator of 5.42 mm was applied to the IVIM maps to match the spatial resolution of the PET images (29). All maps were normalized to MNI space using the same transformation matrix of T1W imaging and the accuracy of image registration were visually inspected. The noise outside the brain was eliminated using the standardized brain map (MNI_152_T1_1mm_brain.nii) from FMRIB's Software Library (FSL) version 5.0 (30). Finally, the cortical infarctions and hemorrhagic lesions were manually deleted from all IVIM and PET maps using MRIcron (http://people.cas.sc.edu/rorden/mricron/index.html) so as not to be included in the regional value analysis. Further, f maps, after deletion of white matter T2 hyperintensities visible on b0 images, were created by applying manually drawn regions of interests (ROI) based on the b0 image to the f map of each patient.
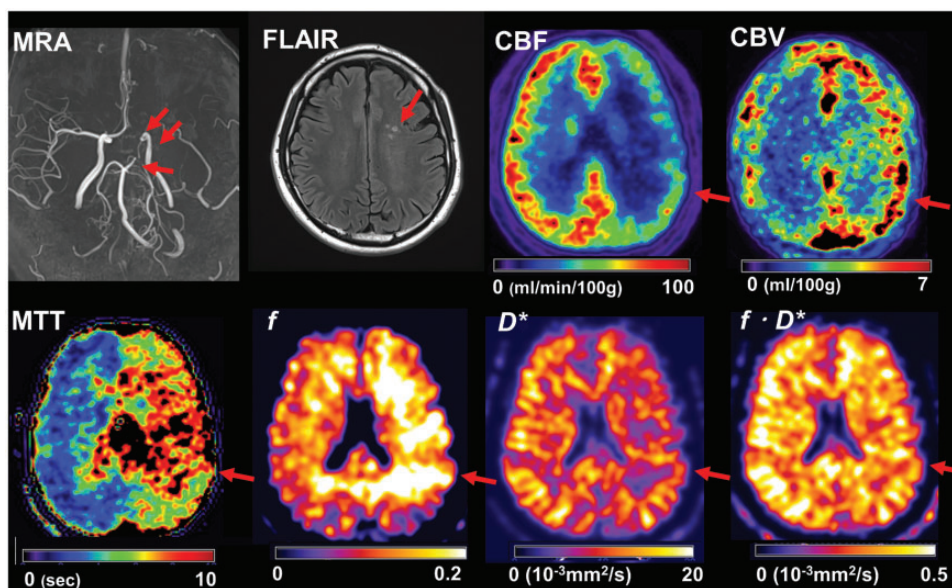

Fig. 1. A 41-year-old man with left unilateral MMD presented with recurrent transient ischemic attack of the right arm. Magnetic resonance angiography (MRA) reveals severe stenosis of the left internal carotid artery, poorly visualized left middle cerebral artery, and the stenotic lesion of posterior cerebral artery (arrows). Several T2 hyperintensities are visualized in the deep white matter of the left hemisphere by fluid-attenuated inversion recovery image (FLAIR, suggested by the arrow). ^{15}O-gas positron emission tomography reveals decreased cerebral blood flow (CBF), increased cerebral blood volume (CBV), and increased mean transit time (MTT) in the left hemisphere (arrows). Smoothed parametric maps of the intravoxel incoherent motion (IVIM) imaging after removal of the noise in the cerebrospinal fluid reveals increased f, decreased D^*, and decreased $f \cdot D^*$ on the left hemisphere compared to the right hemisphere (arrows).
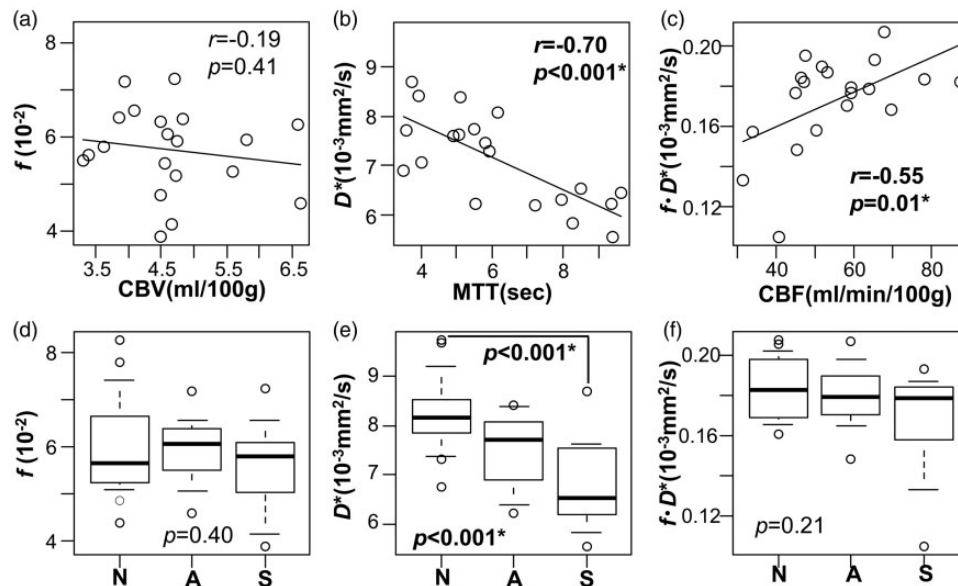
Fig. 2. Comparison of IVIM parametrical values between PET parameters and clinical severity in cortical areas. Although no correlation is observed between f and CBV (a), there is significant negative correlation between D^* and MTT (b) and positive correlation between $f \cdot D^*$ and CBF (c). Significant stepwise trend of increase is observed in D^* as the clinical severity of the hemisphere has increased from N, A to S, as clinically expected (e). There is no significant trend in the f (d) and $f \cdot D^*$ (f) values according to the type of hemisphere. No significant difference was observed among N, A, and S, except for the difference between N and S of D^*. N, normal; A, asymptomatic; S, symptomatic (see "Material and Methods" for details).

ROI analysis

For each map, hemispheric cortical and white matter values were calculated. We used hemispheric cortical and white matter from the Harvard–Oxford cortical and subcortical probabilistic structural atlases (threshold of 25%) distributed with the FSL (31) as ROIs. The ROIs were empirically chosen to appropriately cover the regions of interests (Suppl. Fig. 1). Regional values were calculated using the fsl-stats function of FSL that only consider non-zero voxels; therefore, the deleted lesions in the parametrical maps did not affect the calculated values.

Statistical analysis

All statistical analyses were performed using open source software, EZR version 1.32 (Saitama Medical Center, Jichi Medical University, Saitama, Japan). First, the cortical and white matter values of healthy controls and patients were compared. Then, the correlation between f and CBV, D^* and MTT, and $f \cdot D^*$ and CBF were evaluated, using Pearson correlation test, for both cortical and white matter areas. Further, all IVIM values were categorized into N, A, or S, and evaluated using the Jonckheere-Terpstra trend test and the Tukey-Kramer honest significant difference test. The relationship between f and Fazekas grade, which are considered to correlate with ischemic burden, was

evaluated as well. All results were considered significant when $P < 0.05$.

The full dataset of this study is available from the corresponding author upon reasonable request.

Results

As shown in a representative case (Fig. 1), white matter areas of the f map showed higher values than that of the cortical areas in both the affected and unaffected hemispheres. The average regional values of f, D^*, and $f \cdot D^*$ in the white matter were significantly higher than the values in the cortex ($P < 0.001$ for all).

Although the f values did not correlate with CBV (Figs. 2a and 3a), they were significantly higher in the white matter of patients with MMD than in normal controls (Table 1) and showed significant stepwise change according to the clinical severity of the hemisphere (i.e. from N, A to S; Fig. 3d). The correlation, trend, and difference among the types of hemispheres were essentially the same as those for the analysis of white matter values without deletion of white matter hyperintensities (Suppl. Fig. 3). There was no significant trend or difference in the f values according to the Fazekas grade (Suppl. Tables 2 and 3; $P = 0.95$ for PVH grade; $P = 0.17–0.99$ for DSWMH grade).

The D^* was significantly lower in the cortex of patients with MMD (Table 1) and negatively correlated
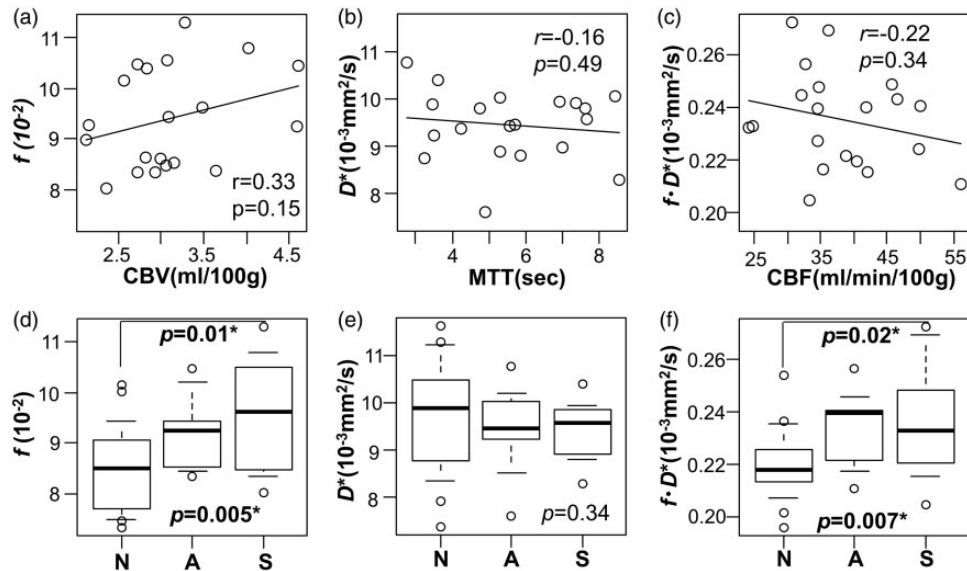
Fig. 3. Comparison of IVIM parametrical values between PET parameters and clinical severity in the white matter areas. No correlation is observed between the parameters of IVIM and those of PET (a–c); f values show significant stepwise trend of increase as the clinical severity of the hemisphere has increased from N, A to S (d); significant trend of change is not observed in D^* (e). The $f \cdot D^*$ values shows significant stepwise trend of increase as the clinical severity of the hemisphere has increased from N, A to S, which is contrary to the clinical expectation (f). No significant difference was observed among N, A, and S, except for the difference between N and S of f and $f \cdot D^*$. CBF, cerebral blood flow; CBV, cerebral blood volume; MTT, mean transit time; N, normal; A, asymptomatic; S, symptomatic (see "Material and Methods" for details).

with MTT (Fig. 2b); however, no correlation was observed between D^* and MTT in the white matter (Fig. 3b).

The $f \cdot D^*$ showed significant positive correlation with CBF in the cortex (Fig. 2c), but not in the white matter (Fig. 3c). In the white matter, $f \cdot D^*$ was significantly higher in patients with MMD than in the controls (Table 1).

Discussion

Although IVIM perfusion might be affected by physiological factors such as cardiac cycle or non-vascular components, previous studies have reported significant correlation between f and the relative CBV measured using DSC was observed in healthy volunteers (8) and patients with tumors or acute stroke (2), as well as between $f \cdot D^*$ and CBF (2). In this study, we found that D^* negatively correlated with MTT, and that $f \cdot D^*$ positively correlated with CBF in the cortical areas, in accordance with the IVIM theory (2,32). Since prolonged MTT is a biomarker of elevated oxygen extraction fraction (15) in patients with MMD, the correlation between MTT and D^* seems promising for its clinical utility.

Unexpectedly, we found no significant correlation between f and CBV, and f values were higher in the white matter area than in the cortex. Theoretically,

f values mainly depend on the flow of arterial, capillary, and venous components (2), as well as PET-measured CBV. Variations in CBV in MMD are quantitated by depicting the difference in the volume of the vessels offering resistance (small arterioles), without influencing the speed of flow. The extremely slow flow in the capillary vessels affects the estimation of the f component, or that the effect of large cortical vessels affecting CBV values was not completely excluded in our ROI analysis; however, this does not explain the high f values in the white matter areas, especially in the symptomatic hemispheres. Larger diffusion kurtosis of the white matter might lead to overestimation of the f values (33). Because the IVIM method quantifies the local diffusion of water molecules, unlike PET or DSC using tracers the f values may be affected by a non-vascular component such as CSF in the parenchyma, which has been increased in symptomatic hemispheres of MMD (34). Measuring the CSF component in a different manner, such as proton density imaging, or measuring the perivascular space or glymphatic system in other methods (35,36) might explain how these components affects the f values and why f values were higher in the white matter than in the cortex.

We also observed higher f values in the white matter areas of patients with MMD than those of healthy controls and a stepwise change in the f values according

to the clinical severity of hemisphere. Increased f and decreased D^* values in white matter hyperintensities (9) and higher f values in the gray matter and the normal-appearing white matter of patients with cerebral small vessel disease than that of normal controls (10) were reported. In PET studies, however, no significant difference between the CBV values in the white matter of patients with and without white matter lesions was reported (37). The results from the analysis of white matter values did not change after deletion of white matter hyperintensities, and there was no significant trend or difference in the f values according to the Fazekas grade; therefore, some other mechanism, such as the disrupted white matter integrity in MMD caused by chronic ischemia (38,39), might lead to the increased f values, as well as other reasons of higher f values in the white matter we discussed previously. The paradoxical results of f values may lead to our paradoxical $f \cdot D^*$ results for the white matter areas. In the cortical areas, the significant correlation between D^* and MTT overcame the poor f-CBV relationship, which may have led to the significant $f \cdot D^*$-CBF correlation.

One serious limitation of this study was the small sample size and the lack of PET data for the healthy volunteers. The use of different software or models would probably produce different results (3); we used commercially available software, considering clinical feasibility. It is unclear if the SNR in this study is enough for D^* measurement (40). Relaxation effects and T2 contribution were not considered; therefore, prolonged T2 of the pathological tissue, which leads to lower f values, may affect the results. We did not perform eddy current correction. We set negative values of IVIM maps to 0 with reference to our previous study; however, this may bias the results, when considering that random fluctuation will result in negative values.

Further investigations are required to establish the clinical feasibility of IVIM for evaluating hemodynamic impairment. Although there are several limitations, this is a unique study investigating the significance of IVIM parameters in comparison with quantitative PET parameters. If the clinical significance of IVIM could be established, its non-invasive nature would be preferential for children and young adults with MMD.

In conclusion, we found significant correlation between D^* and MTT and between $f \cdot D^*$ and CBF, but not between f and CBV; however, higher f values were observed in the white matter of the symptomatic hemispheres compared to the normal hemispheres. Further evaluation is necessary to establish the clinical feasibility of IVIM for the non-invasive evaluation of cerebral perfusion in patients with MMD.

ORCID iD

Shoko Hara 🔟 https://orcid.org/0000-0003-1097-2738

References

1. Le Bihan D, Breton E, Lallemand D, et al. MR imaging of intravoxel incoherent motions: application to diffusion and perfusion in neurologic disorders. *Radiology* 1986;161:401–407.
2. Federau C, O'Brien K, Meuli R, et al. Measuring brain perfusion with intravoxel incoherent motion (IVIM): initial clinical experience. *J Magn Reson Imaging* 2014;39:624–632.
3. Ichikawa S, Motosugi U, Hernando D, et al. Histological grading of hepatocellular carcinomas with intravoxel incoherent motion diffusion-weighted imaging: inconsistent results depending on the fitting method. *Magn Reson Med Sci* 2018;17:168–173.
4. Iima M, Nobashi T, Imai H, et al. Effects of diffusion time on non-Gaussian diffusion and intravoxel incoherent motion (IVIM) MRI parameters in breast cancer and hepatocellular carcinoma xenograft models. *Acta Radiologica Open* 2018;7:2058460117751565.
5. Lecler A, Savatovsky J, Balvay D, et al. Repeatability of apparent diffusion coefficient and intravoxel incoherent motion parameters at 3.0 Tesla in orbital lesions. *Eur Radiol* 2017;27:5094–5103.
6. Kang KM, Choi SH, Kim DE, et al. Application of cardiac gating to improve the reproducibility of intravoxel incoherent motion measurements in the head and neck. *Magn Reson Med Sci* 2017;16:190–202.
7. Calmon R, Puget S, Varlet P, et al. Multimodal magnetic resonance imaging of treatment-induced changes to diffuse infiltrating pontine gliomas in children and

correlation to patient progression-free survival. *Int J Radiat Oncol Biol Phys* 2017;99:476–485.

8. Wu WC, Chen YF, Tseng HM, et al. Caveat of measuring perfusion indexes using intravoxel incoherent motion magnetic resonance imaging in the human brain. *Eur Radiol* 2015;25:2485–2492.

9. Sun J, Yu X, Jiaerken Y, et al. The relationship between microvasculature in white matter hyperintensities and cognitive function. *Brain Imaging Behav* 2017;11:503–511.

10. Wong SM, Zhang CE, van Bussel FC, et al. Simultaneous investigation of microvasculature and parenchyma in cerebral small vessel disease using intravoxel incoherent motion imaging. *Neuroimage Clin* 2017;14:216–221.

11. Federau C, Nguyen A, Christensen S, et al. Cerebral perfusion measurement in brain death with intravoxel incoherent motion imaging. *Neurovascular Imaging* 2016;2:9.

12. Wintermark M, Sesay M, Barbier E, et al. Comparative overview of brain perfusion imaging techniques. *Stroke* 2005;36:e83–99.

13. Guidelines for diagnosis and treatment of moyamoya disease (spontaneous occlusion of the circle of Willis). *Neurol Med Chir (Tokyo)* 2012;52:245–266.

14. Nariai T, Matsushima Y, Imae S, et al. Severe haemodynamic stress in selected subtypes of patients with moyamoya disease: a positron emission tomography study. *J Neurol Neurosurg Psychiatry* 2005;76:663–669.

15. Tanaka Y, Nariai T, Nagaoka T, et al. Quantitative evaluation of cerebral hemodynamics in patients with moyamoya disease by dynamic susceptibility contrast magnetic resonance imaging–comparison with positron emission tomography. *J Cereb Blood Flow Metab* 2006;26:291–300.

16. Hara S, Tanaka Y, Ueda Y, et al. Noninvasive Evaluation of CBF and Perfusion Delay of Moyamoya Disease Using Arterial Spin-Labeling MRI with Multiple Postlabeling Delays: Comparison with 15O-Gas PET and DSC-MRI. *AJNR Am J Neuroradiol* 2017;38: 696–702.

17. Houkin K, Nakayama N, Kuroda S, et al. Novel magnetic resonance angiography stage grading for moyamoya disease. *Cerebrovasc Dis* 2005;20:347–354.

18. Fazekas F, Chawluk JB, Alavi A, et al. MR signal abnormalities at 1.5 T in Alzheimer's dementia and normal aging. *Am J Roentgenol* 1987;149:351–356.

19. Miyatake S, Miyake N, Touho H, et al. Homozygous c.14576G>A variant of RNF213 predicts early-onset and severe form of moyamoya disease. *Neurology* 2012;78:803–810.

20. Miyati T, Imai H, Ogura A, et al. Novel SNR determination method in parallel MRI. *Proc SPIE* 2006;6142:61423O.

21. Nougaret S, Vargas HA, Lakhman Y, et al. Intravoxel incoherent motion–derived histogram metrics for assessment of response after combined chemotherapy and radiation therapy in rectal cancer: initial experience and comparison between single-section and volumetric analyses. *Radiology* 2016;280:446–454.

22. Jerjir N, Bruyneel L, Haspeslagh M, et al. Intravoxel incoherent motion and dynamic contrast-enhanced MRI for differentiation between hepatocellular adenoma and focal nodular hyperplasia. *Br J Radiol* 2017;90:20170007.

23. Neil JJ, Bretthorst GL. On the use of bayesian probability theory for analysis of exponential decay date: an example taken from intravoxel incoherent motion experiments. *Magn Reson Med* 1993;29:642–647.

24. Bettinardi V, Presotto L, Rapisarda E, et al. Physical performance of the new hybrid PETCT Discovery-690. *Med Phys* 2011;38:5394–5411.

25. Shidahara M, Watabe H, Kim KM, et al. Optimal scan time of oxygen-15-labeled gas inhalation autoradiographic method for measurement of cerebral oxygen extraction fraction and cerebral oxygen metabolic rate. *Ann Nucl Med* 2008;22:667–675.

26. Kudomi N, Choi E, Yamamoto S, et al. Development of a GSO detector assembly for a continuous blood sampling system. *IEEE T Nucl Sci* 2003;50:70–73.

27. Shidahara M, Watabe H, Kim KM, et al. Evaluation of a commercial PET tomograph-based system for the quantitative assessment of rCBF, rOEF and rCMRO2 by using sequential administration of 15O-labeled compounds. *Ann Nucl Med* 2002;16:317–327.

28. Federau C, Maeder P, O'Brien K, et al. Quantitative measurement of brain perfusion with intravoxel incoherent motion MR imaging. *Radiology* 2012;265:874–881.

29. Saha GB. *Performance Characteristics of PET Scanners. In: Basics of PET Imaging: Physics, Chemistry, and Regulations*. Cham: Springer International Publishing, 2016:121–142.

30. Jenkinson M, Beckmann CF, Behrens TE, et al. Fsl. *Neuroimage* 2012;62:782–790.

31. Desikan RS, Segonne F, Fischl B, et al. An automated labeling system for subdividing the human cerebral cortex on MRI scans into gyral based regions of interest. *Neuroimage* 2006;31:968–980.

32. Wirestam R, Borg M, Brockstedt S, et al. Perfusion-related parameters in intravoxel incoherent motion MR imaging compared with CBV and CBF measured by dynamic susceptibility-contrast MR technique. *Acta Radiol* 2001;42:123–128.

33. Le Bihan D. What can we see with IVIM MRI? *Neuroimage* 2019;187:56–67.

34. Hara S, Hori M, Inaji M, Maehara T, Aoki S, Nariai T. Regression of White Matter Hyperintensity after Indirect Bypass Surgery in a Patient with Moyamoya Disease. *Magn Reson Med Sci* 2018;ci-2018.

35. Hori M, Fukunaga I, Masutani Y, et al. Visualizing Non-Gaussian Diffusion: Clinical Application of q-Space Imaging and Diffusional Kurtosis Imaging of the Brain and Spine. *Magn Reson Med Sci* 2012;11:221–233.

36. Naganawa S, Nakane T, Kawai H, et al. Gd-based contrast enhancement of the perivascular spaces in the basal ganglia. *Magn Reson Med Sci* 2017;16:61–65.

37. Ibaraki M, Ito H, Shimosegawa E, et al. Cerebral vascular mean transit time in healthy humans: a comparative

study with PET and dynamic susceptibility contrast-enhanced MRI. *J Cereb Blood Flow Metab* 2007;27:404–413.

38. Hara S, Hori M, Murata S, et al. Microstructural Damage in Normal-Appearing Brain Parenchyma and Neurocognitive Dysfunction in Adult Moyamoya Disease. *Stroke* 2018; 49:2504–2507.

39. Conklin J, Fierstra J, Crawley AP, et al. Impaired cerebrovascular reactivity with steal phenomenon is associated with increased diffusion in white matter of patients with Moyamoya disease. *Stroke* 2010;41:1610–1616.

40. Pekar J, Moonen CT, van Zijl PC. On the precision of diffusion/perfusion imaging by gradient sensitization. *Magn Reson Med* 1992;23:122–129.